ADVANCES IN MATERIALS SCIENCE, Vol. 26, No. 1 (87), March 2026

DOI: 10.2478/adms-2026-0003

Piotr Wawrzyniak, Robert Kosturek[1,*], Janusz Torzewski[1], Daniel Klápště[2], Jaromír Moravec[2]

[1]Military University of Technology, Faculty of Mechanical Engineering, 2 gen. S. Kaliskiego str., 00-908 Warsaw, Poland
[2]Technical University of Liberec, Faculty of Mechanical Engineering, Studentská 1402/2 Str., Liberec, Czech Republic

***** *robert.kosturek@wat.edu.pl*

MANUFACTURING OF DISSIMILAR 6061–7075 ALUMINUM ALLOY JOINTS VIA FRICTION STIR WELDING

ABSTRACT

The aim of this study was to investigate the macrostructure, microhardness, and basic mechanical properties of AA6061–AA7075 FSW butt joints produced at different tool rotational speeds (600, 1000, and 1400 rpm) and with offsets toward the AA6061 alloy (0, 1, and 2 mm). The results of the study made it possible to demonstrate that sound, defect-free dissimilar AA6061-T6/AA7075-T6 FSW joints can be produced within the investigated parameter set. The HAZ of the lower-strength alloy was identified as the most critical region of the joint, as confirmed by both microhardness measurements and the fact that all tensile-tested specimens fractured in the HAZ of the 6061-T6 alloy. At the same time, the minimum hardness in this region remained essentially unchanged (approximately 60 HV0.1) across the investigated welding parameters. For joints produced at a constant tool rotational speed of 1000 rpm, increasing the tool offset toward AA6061-T6 reduced weld nugget microhardness due to the increased fraction of the softer alloy in the stirred region, while simultaneously improving elongation at fracture without a noticeable change in tensile strength. Overall, the produced joints exhibited highly repeatable mechanical properties, with joint efficiency in the range of 65–67%.

Keywords: *friction stir welding; welding parameters; mechanical properties; aluminum; dissimilar joints*

INTRODUCTION

Contemporary structural applications of aluminium stem from the combination of low density with the ability to tailor high mechanical performance through alloy design and heat treatment, whose pivotal milestone was the recognition and subsequent practical exploitation of precipitation hardening (age hardening) in high-strength aluminium alloys [1–3]. This strengthening route – typically implemented via solution treatment, quenching, and aging – promotes the formation of fine precipitates that effectively impede dislocation motion, thereby increasing the strength of precipitation-hardenable aluminium alloys [3]. Within aluminium alloy

Received: 02.01.2026; Received in revised form: 11.03.2026; Accepted: 13.03.2026

systematics, the 6XXX and 7XXX series are of particular relevance as precipitation-hardenable systems whose properties depend strongly on temper condition (e.g., T6), which in turn controls both the attainable strength level and the susceptibility to thermal exposure during joining [4,5]. In parallel with alloy/temper selection, recent synthesis work on friction stir welding emphasizes that the thermal–mechanical conditions imposed by the tool (rotation, traverse, axial force and associated heat input) govern the formation of the stir zone and the extent of microstructural transformation, making parameter control central to achieving reproducible quality in both similar and dissimilar joints, as comprehensively reviewed by Sen et al. [6]. Related experimental evidence further shows that even when external heat extraction is modified - e.g., by underwater processing or welding - the altered thermal cycle can measurably change weld morphology and joint performance, underscoring the sensitivity of aluminium joining to boundary conditions, as reported by Janeczek et al. for AA5754 joints produced under underwater FSW regimes [7]. Complementarily, studies on friction-stir-processed high-strength 7XXX alloys indicate that cooling strategy (including air cooling) affects microstructure evolution and the resulting property profile after severe plastic deformation and thermal exposure, which is relevant when translating precipitation-hardenable alloy behavior into robust joining/processing routes; such trends were quantified for 7075 by Iwaszko and Kudła [8]. Consistent with this emphasis on process–property optimization, Hussein et al. show for AA6061-T6 that its weld response is highly sensitive to the selected FSW parameter set, meaning that the alloy's attractive technological characteristics (good weldability and a relatively broad processing window) must still be actively leveraged through controlled heat input and material flow to preserve as much of its temper-derived strength as possible [9].

In this framework, the AA6061-T6/AA7075-T6 material pair constitutes a compelling research case: AA7075-T6 offers very high strength but is frequently constrained by manufacturability and corrosion-related limitations, whereas AA6061-T6 exhibits more favorable weldability and a broader processing window, albeit at lower strength, which motivates the pursuit of joining routes capable of combining the advantages of both alloys in dissimilar joints [5]. At the same time, as discussed in [10], conventional fusion welding of aluminium is hindered by high thermal conductivity, the presence of a stable Al_2O_3 surface film, hydrogen-related porosity, hot cracking, and - critically for precipitation-hardened tempers - property degradation within the heat-affected zone (HAZ), which for 7XXX alloys often translates into a practical restriction of arc-weldability [10]. Against these limitations, the research paper [11] positions friction stir welding (FSW) as particularly suited for joining precipitation-hardenable aluminium alloys because it is a solid-state process (no melting/solidification), which mitigates typical fusion-weld discontinuities (porosity, hot cracking) and commonly reduces the effective width and severity of the HAZ, thereby limiting the extent of strength loss [11]. Consistent with the comparative perspective cited in the research [11], also emphasizes that FSW can yield higher "joint efficiency" (i.e., the ratio of joint tensile strength to the tensile strength of the weaker base material) than conventional TIG/MIG routes across both 6XXX/7XXX precipitation-hardenable alloys and non-heat-treatable systems, which strengthens the case for FSW in high-reliability structures. For dissimilar joints, the central question therefore shifts from mere joinability to controlling the coupled thermal and plastic-flow fields to ensure full plasticization and effective material mixing while minimizing precipitation-strengthening degradation that would otherwise localize the weakest link in the HAZ, a framing that aligns with the synthesis provided by Threadgill et al. as well as with the process-mechanics perspective of Mishra et al. [12,13]. In this respect, AA6061–AA7075 joints represent a model case of dissimilar FSW between alloys with

markedly different flow stresses and plastic responses, where Guo et al. stress the importance of macro-process configuration - specifically the advancing/retreating side arrangement and deliberate tool-axis offset relative to the interface - because FSW flow kinematics are inherently asymmetric and strongly dependent on which alloy is placed on the advancing side [14]. Guo et al. indicate that more favorable mixing is obtained when the lower-flow-stress alloy (AA6061) is positioned on the advancing side, as the more readily plasticized material participates more intensively in the flow, whereas placing the higher-strength alloy on the advancing side increases resistance to deformation and elevates the risk of flow-related defects associated with insufficient fill or disrupted material transport [14]. Additionally, Chen et al. describe tool offset as an engineering lever for altering the relative contribution of each material to the stir zone, since shifting the tool path biases the dominant plasticized stream toward the selected side and can help mitigate phenomena characteristic of dissimilar joints (e.g., compositional non-uniformity in the nugget or interface-adjacent defects) [15].

The selection of thermo-kinematic parameters - especially rotational speed and traverse speed - remains decisive, as they govern heat input per unit length and mixing intensity; accordingly, Seshu Kumar et al. report that increasing rotation rate at fixed traverse conditions can intensify mixing in dissimilar AA6061/AA7075 joints, while Elangovan et al. demonstrate (for AA6061) that rotational speed and tool-pin geometry materially shape joint properties, underscoring why universal “one-direction” rules for strength trends are rarely transferable across tools, fixtures, and thermal boundary conditions [17,18]. Consequently, the literature synthesis motivates treating AA6061–AA7075 FSW not only as a feasibility problem but as a controlled shaping of an asymmetric joint macrostructure (stir zone/nugget, thermo-mechanically affected zone [TMAZ], and HAZ on both sides), in which the HAZ - often on the side of the weaker alloy - exhibits the most pronounced hardness drop and becomes critical for load capacity, thereby governing the attainable joint efficiency in practice [12,15]. The aim of this study is to investigate the effect of tool rotational speed and tool offset on the macrostructure and basic mechanical properties of an AA6061–AA7075 FSW butt joint, addressing a research gap in systematic parameter–structure–property correlations for 6061/7075 dissimilar welds and responding to an industrial need for reliable joining routes that enable hybrid structures combining the high strength of AA7075 with the good manufacturability and weldability of AA6061. The present work addresses a research gap associated with the limited systematic analysis of the combined effects of tool rotational speed and tool offset on the macrostructure and basic mechanical properties of dissimilar AA6061–AA7075 friction stir welded butt joints.

EXPERIMENTAL

The sheets intended for welding were 3 mm thick and were made of the AA6061-T6 and AA7075-T6 alloys, with chemical compositions and mechanical properties presented in the tables below (Tables 1–2). The information presented in the tables comes from the alloy suppliers, namely Alinox Sp. z o.o. (AA6061-T6) and AMAG Rolling (AA7075-T6).

Table 1. *Chemical compositions of welded aluminum alloys*

AA6061-T6								
Si	Fe	Cu	Mn	Mg	Cr	Zn	Ti	Al
0.62	0.4	0.18	0.1	1.0	0.07	0.05	0.07	Base
AA7075-T6								
Si	Fe	Cu	Mn	Mg	Cr	Zn	Ti	Al
0.06	0.12	1.6	0.03	2.6	0.19	5.8	0.05	Base

Table 2. *Mechanical properties of welded aluminum alloys*

AA6061-T6		
Yield Strength (YS)	Tensile Strength (UTS)	Elongation (A)
255 MPa	290 MPa	12%
AA7075-T6		
Yield Strength (YS)	Tensile Strength (UTS)	Elongation (A)
515 MPa	583 MPa	12%

The joints were produced on an ESAB Legio 4 UT machine, using an ESAB 20/09 SA high-speed steel tool with a flat shoulder 16 mm in diameter at its base and a threaded, conical pin with a diameter of 6.8 mm at the shoulder interface and 5 mm at the tip, and a height of 2.7 mm. Before joining, the sheet edges were milled, and the upper surfaces were cleaned of oxides with abrasive paper and then degreased with acetone. Based on the findings of J.F. Guo et al. concerning dissimilar FSW joints of 6061 and 7075 alloys (at a constant tool rotational speed of 1200 rpm), it was concluded that material mixing is more favorable when the 6061 alloy is placed on the advancing side. This is attributed to the markedly lower flow stress of 6061 compared with 7075 (19.8 vs 56.3 N/mm²). In dissimilar FSW, positioning the lower-strength material on the advancing side promotes plastic deformation and improves material flow, whereas placing the stronger alloy on the advancing side increases resistance to deformation, hinders material distribution, and reduces the likelihood of obtaining a defect-free joint [14]. For this reason, in this study, it was decided to place the 7075-T6 alloy on the retreating side and the 6061-T6 alloy on the advancing side, considering this arrangement to be the most optimal for the strength properties of the obtained joints. The welding setup used is shown in Figure 1.

The influence of the FSW parameters on the properties of the obtained joints was investigated by comparing five different variants of selected welding parameters. The set of analyzed specimens can be divided into two groups as follows: without offset and with an offset applied toward the 6061-T6 alloy. In the first group, the distinguishing criterion was the tool rotational speed, for which the following values were adopted, respectively: 600, 1000, 1400 rpm. In the second group, the joints were produced at a constant rotational speed of 1000 rpm, selecting the following offset values in turn: 0, 1, 2 mm. One of the joint variants (1000 rpm and 0 mm offset) can be classified into both groups. It was decided to adopt a constant tool traverse speed of 125 mm/min and a plunge depth of 2.8 mm for all joints, limiting the parameter control

solely to the tool rotational speed and the offset. The tool tilt angle was two degrees. The applied welding parameters, together with the specimen designations, are summarized in Table 3.

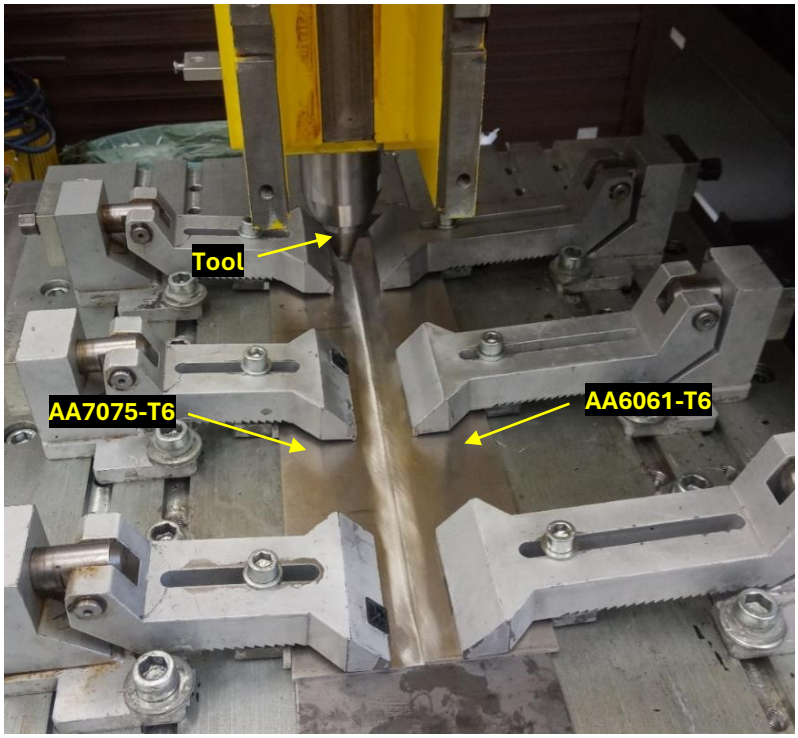

Fig. 1. Applied welding system

Table 3. *Welding parameters and sample designation*

Sample designation	Tool rotation speed [rpm]	Offset toward AA6061 [mm]	Tool penetration depth [mm]	Welding velocity [mm/min]
R6	600	0	2.8	125
B	1000			
R14	1400			
P1	1000	1		
P2		2		

After welding, the specimens were sectioned perpendicular to the welding direction and prepared for metallographic examination by resin mounting, grinding, and polishing. To reveal the grain structure, the prepared surfaces were etched for 10 s in Keller's reagent (20 mL H_2O + 5 mL HNO_3 + 1 mL HCl + one drop of HF) and then examined using an Olympus LEXT OLS 4100 digital light microscope. Vickers microhardness profiles were measured on a Struers DuraScan system using a 0.98 N load along a line located 1.5 mm below the weld face. Tensile testing was carried out on an INSTRON 8802 MTL machine using an extensometer with a 50 mm gauge length. The schematic of the specimen for the static tensile test is shown below in Figure 2.

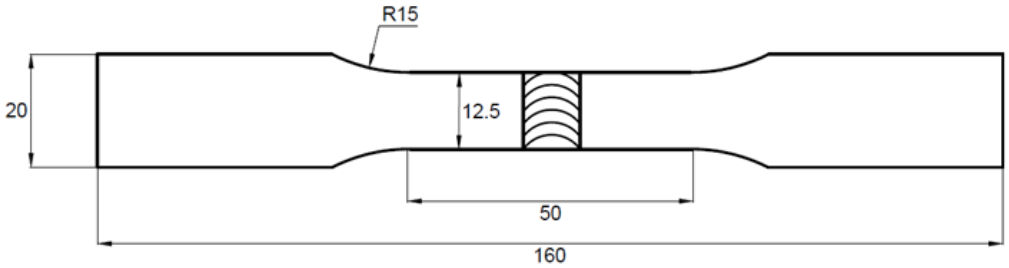

Fig. 2. Geometry of the tensile test specimen

All tests were carried out three months after the joining process in order to allow the mechanical properties of the joint to stabilize before testing. For each welded joint, three tensile tests were performed.

RESULTS AND DISCUSSION

The first stage of the study focused on observations of the macrostructure of the obtained joints. Etching the specimens with Keller's reagent enabled the AA7075 alloy to be revealed, while it did not affect the AA6061 alloy, which made it possible to accurately observe the presence and distribution of both materials within the joint zone. The macrostructural images are presented in Figure 3.

As part of the macrostructural analysis of all cross-sections, no joint defects, such as a remnant joint line or voids, were observed. In addition, the joints were successfully produced through the entire joining depth. In the joints produced at different tool rotational speeds (Fig. 3 R6, B, R14), an increase in weld nugget volume can be observed with increasing rotational speed. Although the width of the weld nugget base appears to remain unchanged, a clearly visible feature affecting the nugget volume is its "narrowing" toward the retreating side, i.e., the 7075-T6 alloy. As the tool rotational speed increases, this curvature becomes less pronounced. At lower rotational speed (Fig. 3 R6), a smaller fraction of the 6061-T6 alloy placed on the advancing side is also visible in the central part of the joint (the darker color appears more frequently). The increased rotational speed provided better mixing of both materials, as evidenced by the darker curved bands (7075-T6 material intrusions), caused by the circular material flow, in the central part of the weld nugget in samples B and R14. In the weld nuggets of all analyzed cases, a characteristic material distribution can be observed, referred to in the literature as "onion rings". In joint R6, these rings are much more distinct on the advancing side. In the remaining joints, no such difference is observed. This asymmetry in joint R6 may be explained by the different flow trajectories of the materials placed on opposite sides, which become apparent at the specific, here relatively low, tool rotational speed [18].

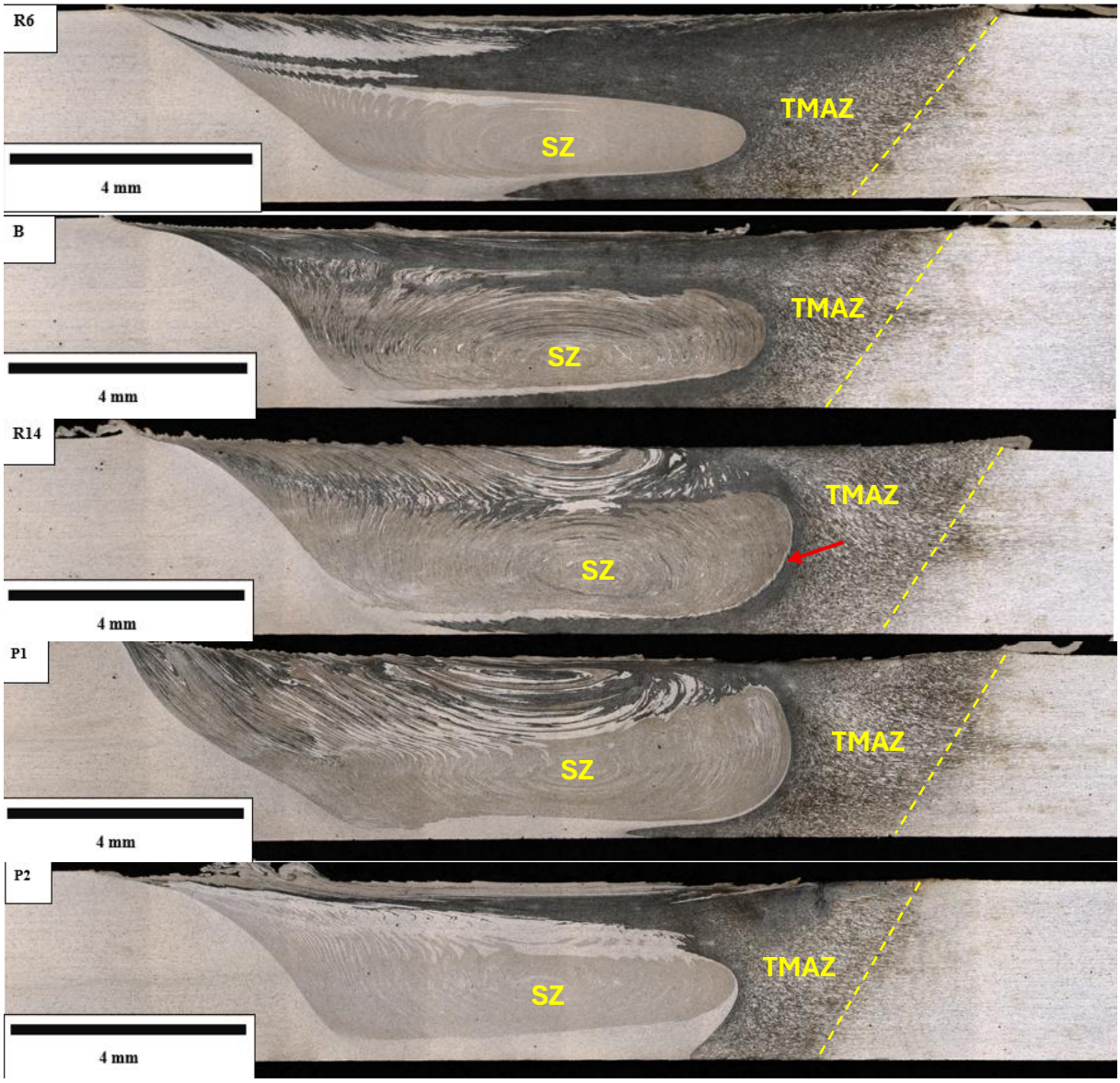

Fig. 3. Macrostructural images of the produced joints (etched AA7075-T6 alloy). The stir zone (SZ) and the thermo-mechanically affected zone (TMAZ) in the 7075-T6 alloy are marked, together with the boundary between the TMAZ and HAZ indicated by the yellow dashed line. The red arrow is described in the text

For all cross-sections, the weld nugget is "seated" on a thin band of 6061-T6 material. A particularly interesting observation is that, in joint R14 (see the red arrow in Fig. 3, R14), this band forms the boundary between the weld nugget and the 7075-T6 alloy, as if it were "driven" between them. In the authors' view, one possible explanation of this phenomenon may be the observation that, in the joining zone, the lower parts of the material are set into motion last and therefore heat up more slowly than the upper regions [19]. In other words, the temperature gradient increases with the height of a given point in the joining zone. The tool first interacts with the upper portions of the material, and consequently, the direct contact with the tool shoulder and the resulting friction cause these upper regions to reach the highest temperature [20]. Although these differences must be small, it is possible that they affect the distribution of material located

at the very bottom. It is likely that the final rotation of the tool pin at a given cross-sectional location constitutes the last "pickup" of the final, unmixed layer of material from the advancing side, which then appears to penetrate between the weld nugget and the TMAZ on the retreating side. It should also be noted that this phenomenon is to some extent dependent on the tool rotational speed and tool pin shape.

As can be seen from the analyzed images, changes in tool rotational speed affect the appearance of the region in direct contact with the tool shoulder (the shoulder-driven zone). In samples R6 and B, this region is dominated by the alloy placed on the retreating side (a much greater fraction of the darker color). A tendency can be observed that, with increasing tool rotational speed, the mixing of materials increases, and this first becomes visible from the advancing side (from left to right). An increase in the volume of the TMAZ (especially for the 7075-T6 alloy) with increasing tool rotational speed is also apparent. In the image of sample R14, the grains appear to be deformed over a larger area than in the corresponding image of sample R6, which is visible in the upper part of the TMAZ on the advancing side of that sample.

As part of the macrostructural analysis of the specimens welded with an offset (Fig. 3, P1 and P2), no major defects indicating a non-optimal selection of welding parameters were observed. Shifting the tool relative to the line defining the interface between the joined materials toward the 6061-T6 alloy has a significant effect on the fraction of 7075-T6 alloy present in the joint. In both images, a reduced intensity of the darker color can be observed in the weld nugget. This fraction is the lowest in specimen P2. An interesting consequence of the applied offset is the lack of a clearly visible regularity in the manner and direction of weld nugget deformation with increasing offset value. It is sufficient to note that specimen B (no offset) differs substantially from specimen P1. Similarly, specimen P2 differs in appearance from P1. In joint P1, the boundary between the weld nugget and the TMAZ on the advancing side is distorted relative to the other specimens. In this joint, greater material mixing is visible in the tool shoulder interaction zone than in specimen B. Specimen P2 is characterized by the lowest fraction of 7075-T6 alloy in the joint - the material from the retreating side is distributed over a smaller area of the tool shoulder interaction zone than in specimen R6. Increasing the offset from 1 mm to 2 mm in specimen P2 resulted in a sudden change in the curvature of the weld nugget on both sides relative to specimen P1. Specimens P1 and P2 share a visible asymmetry in the curvature of the onion rings; they differ in that this curvature is greater on the advancing side and smaller on the retreating side in joint P1, whereas the opposite is observed in P2.

In the next stage of the study, microhardness measurements were performed for the obtained joints, and the resulting distributions are presented in Fig. 4a,b.

A noticeable asymmetry can be observed between the hardness values of the two joined alloys. The hardness in the weld region to the right of its center remains relatively close to that of the material located on the retreating side; similarly, on the left side, it remains close to that of the material located on the advancing side. However, in the weld nugget - the zone most susceptible to mixing of both materials - the hardness value is (to a greater or lesser extent) closer to that of the softer material (6061-T6). When analyzing the effect of tool rotational speed on the microhardness distribution in the joint (Fig. 4a), it can be observed that the microhardness of the weld nugget increases with increasing rotational speed. It reaches approximately 60 HV0.1 at 600 rpm, approximately 80 HV0.1 at 1000 rpm, and approximately 86 HV0.1 at 1400 rpm. An increase in tool rotational speed raises the amount of heat generated during the FSW process, which results, among other effects, in a wider heat-affected zone and lower hardness in the low-

hardness zone [13]. This is reflected in the present results, particularly in terms of the width of the HAZ in the AA6061-T6 alloy, which extended to approximately 10, 12, and 15 mm from the joint line with increasing tool rotational speed. At the same time, within the investigated parameter range, no significant effect of tool rotational speed on the minimum hardness recorded in the joint was observed.

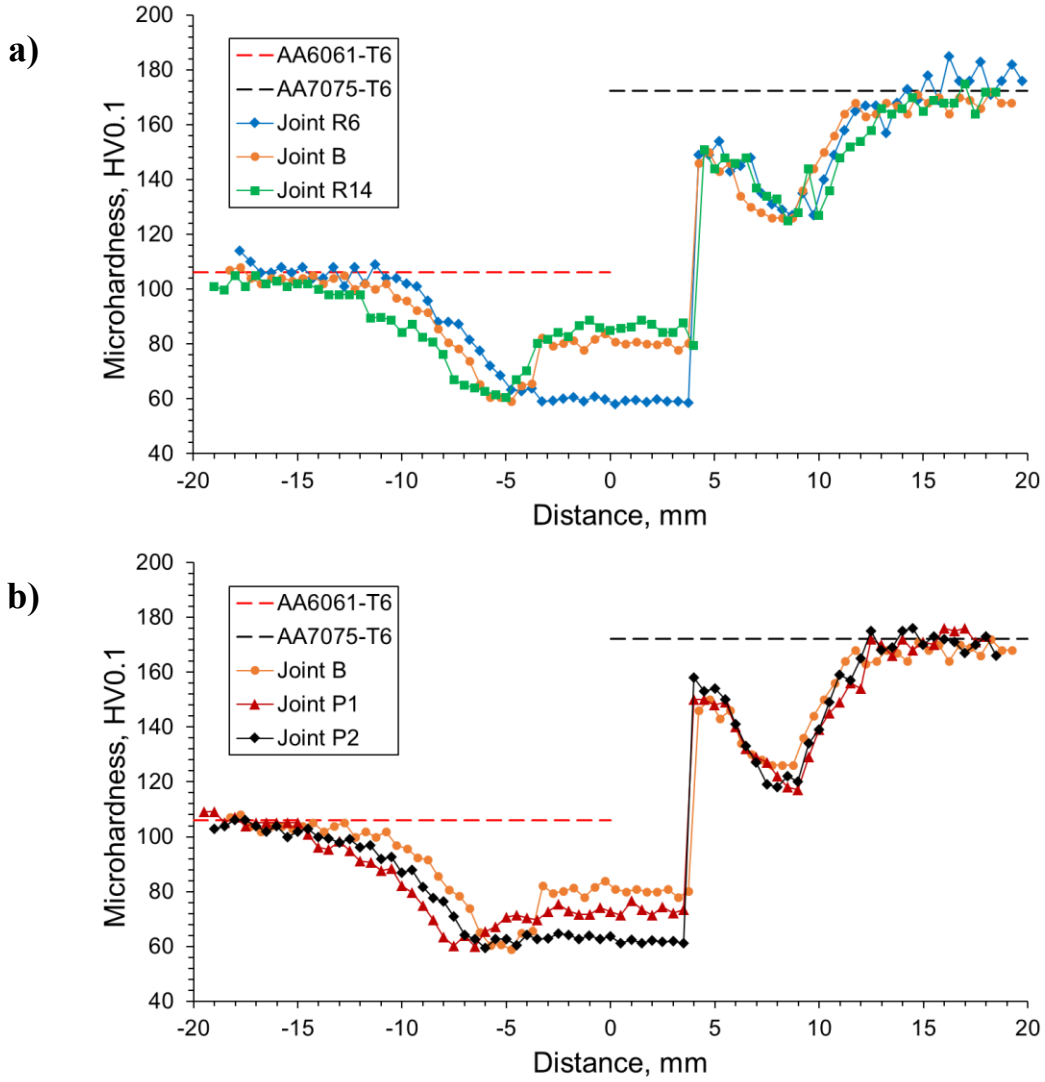

Fig. 4. Microhardness distributions of joints obtained at different tool rotational speeds (a) and different offset values (b)

Simultaneously, it was found that shifting the tool offset toward the AA6061-T6 alloy at a constant rotational speed of 1000 rpm (Fig. 4b) causes a significant decrease in the microhardness of the weld nugget, directly related to the greater fraction of the softer alloy in the stirred region. Microhardness in this region decreases from 80 HV0.1 (offset 0) to approximately 74 HV0.1 (offset 1) and 63 HV0.1 (offset 2).

A significant decrease in hardness, characteristic of precipitation-hardened aluminum alloys, is observed when moving from the base material toward the weld center. For both alloys, the hardness profile as a function of distance from the joint center resembles half of a "W"-shaped distribution; however, this pattern is observed only for samples B, R14, and P1. In these joints, the minimum hardness was recorded in the HAZ of the 6061-T6 alloy and remained within a comparable range (approximately 58.7–61.2 HV0.1). This suggests that, within the investigated parameter window, tool rotational speed and offset do not directly affect the minimum hardness in the HAZ of the softer alloy placed on the advancing side. A different trend was observed for samples R6 and P2. Although the most pronounced hardness reduction still occurred on the advancing side, the minimum hardness was recorded in the weld nugget. However, the difference between the hardness in the HAZ on the advancing side and that in the weld nugget was small and may fall within the measurement uncertainty. Therefore, for general interpretation, the HAZ on the advancing side may still be regarded as the critical low-hardness region, provided that the softer alloy is located on that side. In samples R6 and P2, no hardness recovery was observed in the TMAZ on the advancing side or in the weld nugget relative to the reduced hardness level in the HAZ. Instead, the hardness remained close to the minimum value recorded in the HAZ on the advancing side as the measurement path approached the weld center. This behavior is consistent with the macrostructural observations (Fig. 3), which indicated a low fraction of 7075-T6 in the weld nugget, suggesting limited material mixing under the selected processing conditions. Accordingly, the hardness profiles of R6 and P2 support the conclusion that a reduced fraction of 7075-T6 in the joint lowers the hardness of both the weld nugget and the TMAZ on the advancing side, i.e., regions that would otherwise be more strongly affected by 7075-T6 under more effective mixing conditions. It should also be emphasized that a complete assessment of the influence of process parameters on weld nugget microhardness requires consideration of post-weld precipitation phenomena and the natural aging potential of the weld nugget as a function of applied tool rotational speed and offset [21].

Representative tensile curves of the base materials and FSW joints are shown in Fig. 5, while the determined values of mechanical parameters and fracture locations are summarized in Table 4.

Regardless of changes in tool rotational speed (Fig. 5a) or the applied offset (Fig. 5b), no significant effect on the mechanical properties of the FSW joints was observed. The tensile strength of the obtained joints remains at a similar level (approximately 220-225 MPa, corresponding to a joint efficiency of about 66%), which indicates that, within the investigated range, tool rotational speed and the applied offset toward the alloy located on the advancing side have, by themselves, only a marginal effect on the overall strength parameters of the joint. The joint efficiencies also remain at a comparable level. The obtained strength parameter results, due to their relatively similar values and standard deviations, do not allow for drawing broader conclusions regarding the effect of tool rotational speed on YS and UTS. According to the data reported in the literature, the effect of rotational speed on joint strength is nonlinear — increasing the tool rotational speed improves the mechanical properties only up to a certain optimum, beyond which they deteriorate [13]. In the present study, despite the relatively wide range of rotational speeds applied, the occurrence of such a relationship cannot be stated with certainty.

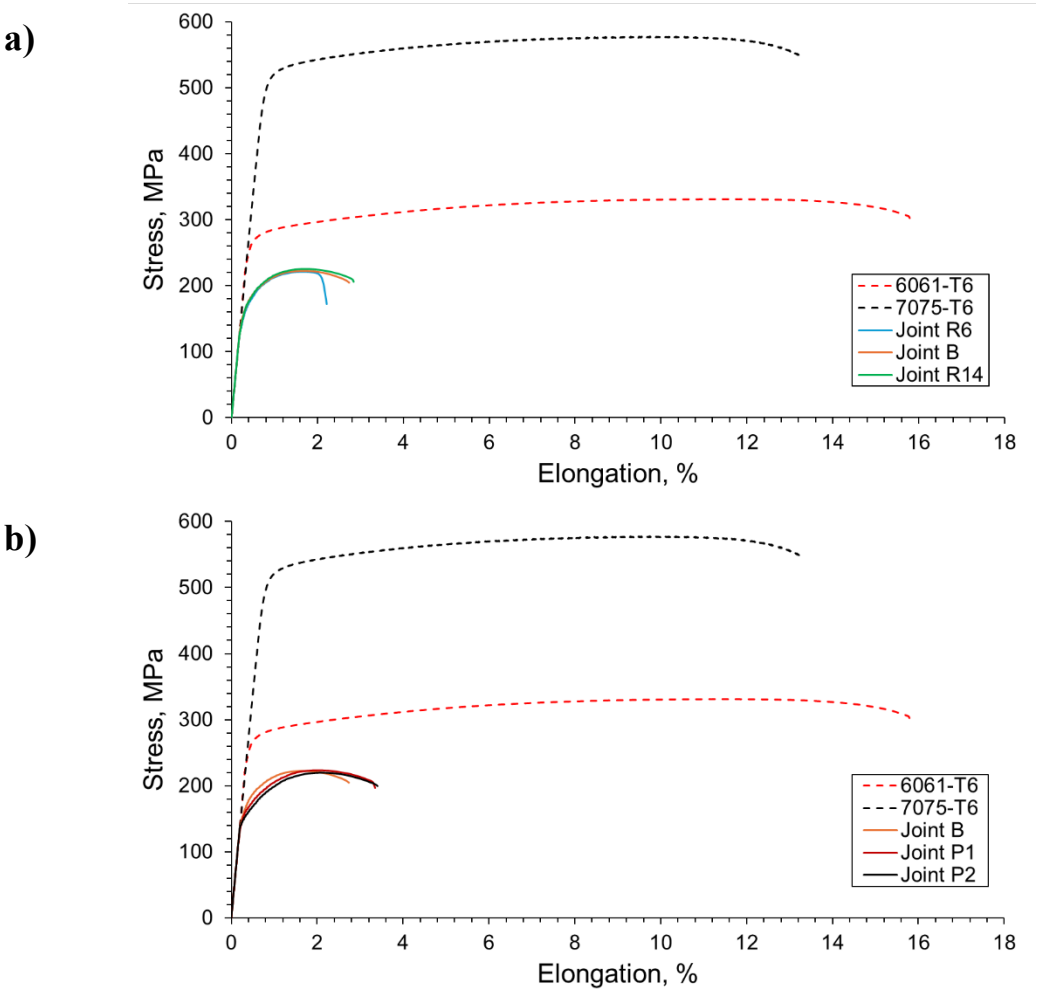

Fig. 5. Stress-strain curves of joints obtained at different tool rotational speeds (a) and different offset values (b)

Table 4. *The established mechanical properties and failure location*

Joint	YS [MPa]	UTS [MPa]	Joint efficiency [%]	Failure
R6	182.4 ± 12.9	225 ± 5.2	67	HAZ (6061-T6)
B	184.4 ± 1	220.1 ± 2.5	65	
R14	183.9 ± 1.3	224.3 ± 1.4	67	
P1	172.5 ± 2.9	224.2 ± 1.2	67	
P2	167.2 ± 5.1	220.6 ± 1.8	66	

The only apparent difference between the investigated samples is the higher elongation at fracture observed for the joints produced with an applied offset, i.e., P1 and P2. The results indicate that an increased fraction of the AA6061 alloy led to a higher elongation at fracture, while not reducing the tensile strength. All analyzed specimens failed in the HAZ of the AA6061-T6 alloy (Table 4), corresponding to the region in which an approximately 40% reduction in the microhardness of this material was observed (Fig. 4a,b), making it the weakest

area of the produced joints. The marginal effect of offset toward the AA6061 alloy, within the investigated parameter range, on the properties of the produced joints may be interpreted positively in the context of potential inaccuracies in tool positioning during the production process, as such inaccuracies do not have a noticeable effect on joint quality. The obtained joint-efficiency values are slightly lower than those reported in the study [14] and are also markedly below the efficiencies achieved for similar (same-alloy) precipitation-hardened aluminum joints such as AA2519-T62 [22] or AA7075-T651 [23].

The present results align well with prior reports on 6061/7075 FSW joints. The dominant softening on the AA6061-T6 side - reflected by the hardness minimum and the tensile fracture location in/near the 6061 HAZ - is consistent with the localized deformation and failure behavior described by Suthar et al. [24]. For the tested parameter/offset variants, the limited changes in strength can be rationalized in line with Liu et al. [25], i.e., similar effective heat input and material-flow conditions leading to comparable mixing and nugget strengthening. At the same time, the higher elongation observed for the offset condition agrees with the trends reported by Seshu Kumar et al. [26], where tool positioning can improve ductility without proportionally increasing UTS when failure remains HAZ-controlled. Finally, literature indicates that mechanical post-processing (e.g., deep rolling) may further enhance the performance of such joints [27], while microstructure evolution in the softened zones may also affect electrochemical response [28], motivating complementary corrosion-focused assessment.

In this work, the tool offset was applied only toward the AA6061 side to promote process stability and defect-free bonding, given the broader processing window of the 6xxx alloy. However, this deliberately limits the scope, since offset strongly governs material flow, heat distribution, and the location/extent of softening in dissimilar 6061/7075 joints. Future work should therefore systematically investigate offset toward AA7075 to better quantify its influence on macrostructure, hardness profiles, joint efficiency, and failure mode, especially considering the high strength and process sensitivity of AA7075-based joints reported for friction-based welding of 7075 alloys [29-31]. In parallel, post-weld heat-treatment routes should be assessed because they can substantially modify microstructure and mechanical response in AA7075-containing friction stir joints [32]. This continuation is also consistent with recent optimization-oriented studies emphasizing the critical role of tool positioning and material flow control in dissimilar aluminum friction-based joining [33], underlining that the optimization of process parameters is a key factor in balancing heat input, material mixing, and microstructural development [34], and thus in obtaining joints with reliable mechanical properties [35-36].

CONCLUSIONS

The following conclusions can be drawn from this study:

1. Within the investigated parameter set (tool rotational speeds: 600, 1000, and 1400 rpm; tool offset toward AA6061: +0, +1, and +2 mm), defect-free dissimilar AA6061-T6/AA7075-T6 joints were successfully produced, confirming that the selected welding conditions provide a suitable processing window for obtaining sound butt joints in this material system.
2. The HAZ of the lower-strength alloy was identified as the most critical region of the FSW joint, as confirmed by microhardness measurements and by the fact that all tensile-tested joints fractured in the HAZ of the 6061-T6 alloy, while the minimum hardness in this region remained essentially unchanged (approx. 60 HV0.1) across the investigated welding

parameters. This indicates that, despite changes in tool rotational speed and tool offset, the local softening of the AA6061-T6 side governs the tensile failure behavior of the joint.

3. At a constant tool rotational speed of 1000 rpm, increasing the tool offset toward the AA6061-T6 alloy reduced weld nugget microhardness as a result of the increased fraction of the softer alloy in the stirred region, while simultaneously improving elongation at fracture without a noticeable change in tensile strength. This demonstrates that tool offset can be used to modify the local structure–property balance of the weld, particularly in terms of hardness and ductility.
4. The produced joints exhibited highly repeatable mechanical properties, with joint efficiency in the range of 65–67%, indicating good process stability within the investigated parameter range despite the material asymmetry of the dissimilar AA6061-T6/AA7075-T6 configuration.
5. More broadly, the results contribute to filling the research gap related to the still limited systematic understanding of the combined effects of tool rotational speed and tool offset on the macrostructure and basic mechanical properties of dissimilar AA6061–AA7075 friction stir welded butt joints. In particular, the study shows that within the applied parameter range, these variables affect weld-region hardness distribution and ductility more distinctly than ultimate tensile strength or joint efficiency, while the softened HAZ of the AA6061-T6 alloy remains the dominant factor controlling joint performance.

ACKNOWLEDGEMENT

This work was financed by Military University of Technology under the research project UGB 531-000104-W100-22.

Conflicts of Interest

The authors declare that they have no competing financial interests or personal relationships that could have seemed to influence the study reported in this paper.

REFERENCES

1. Polmear I.J.: Aluminium alloys – a century of age hardening. Materials Forum 28 (2004), 1–14.
2. Merica P.D., Waltenberg R.G., Scott H.: Heat treatment of duralumin. Scientific Papers of the Bureau of Standards 15 (1919–1920), 271–316.
3. Fine M.E.: Precipitation hardening of aluminum alloys. Metallurgical Transactions A 6 (1975), 625–630.
4. Askeland D.R.: The Science and Engineering of Materials. Springer/Chapman & Hall, New York, 1996.
5. Hatch J.E.: Aluminum: Properties and Physical Metallurgy. J.E. Hatch [ed.], Aluminum Association Inc. & ASM International, 1984.

6. Sen M., Ozcan M.E., Yildiz Y.O., Aver M., Kapan S., Huseyinoglu M., Yigid O., Kara S.E.: A Comprehensive Study on Friction Stir Welding: A Review. Soldagem & Inspeção 30 (2025), e3016.
7. Janeczek A., Tomków J., Derazkola H.A., Łyczkowska K., Fydrych D.: Effect of underwater friction stir welding parameters on AA5754 alloy joints: experimental studies. The International Journal of Advanced Manufacturing Technology 134(11) (2024), 5643–5655.
8. Iwaszko J., Kudła K.: Evolution of Microstructure and Properties of Air-Cooled Friction-Stir-Processed 7075 Aluminum Alloy. Materials 15(7) (2022), 2633.
9. Hussein A.K., Barrak O.S., Hamzah M.M., Hussein S.K.: Friction stir welding AA6061-T6 with multi-objective optimization of parameters. Advances in Science and Technology Research Journal 19(10) (2025), 162–172.
10. Kou S.: Welding Metallurgy. John Wiley & Sons, Hoboken, 2002.
11. Mathers G.: The Welding of Aluminium and its Alloys. Woodhead Publishing, Cambridge, 2002.
12. Threadgill P.L., Leonard A.J., Shercliff H.R., Withers P.J.: Friction stir welding of aluminium alloys. International Materials Reviews 54(2) (2009), 49–93.
13. Mishra R.S., Mahoney M.W.: Friction Stir Welding and Processing. ASM International, 2007.
14. Guo J.F., Chen H., Sun C., Bi G., Sun Z., Wei J.: Friction stir welding of dissimilar materials between AA6061 and AA7075 Al alloys: effects of process parameters. Materials & Design 56 (2014), 185–192.
15. Liang Z., Chen K., Wang X., Yao J., Yang Q., Zhang L., Shan A.: Effect of Tool Offset and Tool Rotational Speed on Enhancing Mechanical Property of Al/Mg Dissimilar FSW Joints. Metallurgical and Materials Transactions A 44A (2013), 3721–3731.
16. Seshu Kumar G.S.V., Kumar A., Rajesh S., Chekuri R.B.R., Ramakotaiah K.: Optimization of FSW process parameters for welding dissimilar 6061 and 7075 Al alloys using Taguchi design approach. International Journal of Nonlinear Analysis and Applications 13(1) (2022), 1011–1022.
17. Elangovan K., Balasubramanian V., Valliappan M.: Effect of Tool Pin Profile and Tool Rotational Speed on Mechanical Properties of Friction Stir Welded AA6061 Aluminium Alloy. Materials and Manufacturing Processes 23(3–4) (2008), 251–260.
18. Khodir S.A., Shibayanagi T.: Microstructure and Mechanical Properties of Friction Stir Welded Dissimilar Aluminum Joints of AA2024-T3 and AA7075-T6. Materials Transactions 48(7) (2007), 1928–1937.
19. Kalashnikova T., Chumaevskii A., Kalashnikov K., Fortuna S., Kolubaev E., Tarasov S.: Microstructural Analysis of Friction Stir Butt Welded Al-Mg-Sc-Zr Alloy Heavy Gauge Sheets. Metals 10(6) (2020), 806.
20. Cui S., Chen Z.W.: Effects of tool speeds and corresponding torque/energy on stir zone formation during friction stir welding/processing. IOP Conference Series: Materials Science and Engineering 4(1) (2009), 012019.
21. Kalemba I., Kopyściański M., Hamilton C., Dymek S.: Natural Aging Behavior Of Friction Stir Welded Al-Zn-Mg-Cu Aluminum Alloys. Archives of Metallurgy and Materials 60(2) (2015), 875–879.
22. Kosturek R., Ślęzak T., Torzewski J., Wachowski M., Śnieżek L.: Study on tensile and fatigue failure in the low-hardness zone of AA2519-T62 FSW joint. Manufacturing Review 9 (2022), 25.

23. Kosturek R., Lewczuk R., Torzewski J., Wachowski M., Słabik P., Maranda A.: Research on the post-weld explosive hardening of AA7075-T651 friction stir welded butt joints. Bulletin of the Polish Academy of Sciences: Technical Sciences 71(4) (2023), e145685.

24. Suthar H., Bhattacharya A., Paul S.K.: Local deformation response and failure behavior of AA6061–AA6061 and AA6061–AA7075 friction stir welds. CIRP Journal of Manufacturing Science and Technology 30 (2020), 12–24.

25. Liu S., Ren Y., Hu X.: Characterization of microstructure and mechanical properties of dissimilar FSW joints of 7075/6061 aluminum alloys: The effects of welding heat input and material flow behavior. Structures 80 (2025), 110030.

26. Seshu Kumar G.S.V., Kumar A., Rajesh S., Chekuri R.B.R., Ramakotaiah K.: An experimental study and parameter optimization of FSW for welding dissimilar 6061 and 7075 Al alloys. International Journal on Interactive Design and Manufacturing (IJIDeM) 17 (2023), 215–223.

27. Kaewkham P., Nakkiew W., Baisukhan A.: Mechanical properties enhancement of dissimilar AA6061-T6 and AA7075-T651 friction stir welds coupled with deep rolling process. Materials 15(18) (2022), 6275.

28. Lipińska M., Kooijman A., Śnieżek L., Szachogłuchowicz I., Torzewski J., Gonzalez-Garcia Y., Lewandowska M.: The Influence of Microstructure Evolution on the Mechanical and Electrochemical Properties of Dissimilar Welds from Aluminum Alloys Manufactured Via Friction Stir Welding. Metallurgical and Materials Transactions A 55 (2024), 4373–4390.

29. Kluz R., Kubit A., Wydrzyński D.: Analysis of Structure and Shear/Peel Strength of Refill Friction Stir Spot Welded 7075-T6 Aluminium Alloy Joints. Advances in Science and Technology Research Journal 11(3) (2017), 297–303.

30. Kluz R., Kubit A., Trzepiecinski T., Faes K.: Polyoptimisation of the Refill Friction Stir Spot Welding Parameters Applied in Joining 7075-T6 Alclad Aluminium Alloy Sheets Used in Aircraft Components. The International Journal of Advanced Manufacturing Technology 103 (2019), 3443–3457.

31. Kubit A., Trzepieciński T., Gadalińska E., Slota J., Bochnowski W.: Investigation into the Effect of RFSSW Parameters on Tensile Shear Fracture Load of 7075-T6 Alclad Aluminium Alloy Joints. Materials 14 (2021), 3397.

32. Kumar R., Upadhyay V., Pandey C.: Effect of post-weld heat treatments on microstructure and mechanical properties of friction stir welding joints of AA2014 and AA7075. Journal of Materials Engineering and Performance 32(24) (2023), 10989–10999.

33. Kumaran Selvaraj S., Manoj A.L., Mathew A.B., Govind A.V., Sundaramali G., Chadha U., Vajipeyajula B., Patterson A.E.: Parameter Optimization for Dissimilar Aluminum Alloys Joined Using Friction Stir Additive Manufacturing: A Screening Study. Engineering Reports 7(1) (2025), e13039.

34. Szala M., Walczak M., Pałka T., Kowal M., Nowak W.J.: Comparison of cavitation erosion and sliding wear resistance of welded CoCrWC and NiCrBSi hardfacings, AISI 316L stainless steel, and S235JR mild steel. Advances in Science and Technology Research Journal 19 (2025), 275-291.

35. Kubit A., Trzepieciński T., Kluz R., Ochałek K., Slota J.: Multi-Criteria Optimisation of Friction Stir Welding Parameters for EN AW-2024-T3 Aluminium Alloy Joints. Materials 15 (2022), 5428.

36. Kluz R., Kubit A., Trzepiecinski T., Faes K., Bochnowski W.: A Weighting Grade-Based Optimization Method for Determining Refill Friction Stir Spot Welding Process Parameters. Journal of Materials Engineering and Performance 28 (2019), 6471–6482.